Detection of nickel atom by laser induced fluorescence during carbon nanotube formation in a laser produced plume

G. De Boer[a)]
Department of Chemistry and Physics, LeTourneau University, 2100 South Mobberly, Longview, Texas 75602

S. Arepalli, W. Holmes, and P. Nikolaev
G. B. Technology/NASA-JSC, Mail Stop ES42, 2100 NASA Road One, Houston, Texas 77058

C. Range
Department of Chemistry and Physics, LeTourneau University, 2100 South Mobberly, Longview, Texas 75602

C. Scott
NASA/JSC, 2100 NASA Road One, Mail Stop ES3, Houston, Texas 77058

(Received 14 August 2000; accepted for publication 21 February 2001)

In situ monitoring of catalyst nickel atoms by laser induced fluorescence during carbon nanotube formation in a laser-produced plume was performed at the Johnson Space Center nanotube production laboratory. The results indicate that ablation of nickel and plume dynamics are strongly related to the oven temperature. Nickel atoms have a long lifetime of several milliseconds and have an electronic temperature of at least 1500 K during carbon nanotube formation. © *2001 American Institute of Physics.* [DOI: 10.1063/1.1365441]

I. INTRODUCTION

The mechanism of carbon nanotube formation and the role of the metal catalysts have been an intriguing topic since the discovery of carbon nanotubes.[1] Although computational efforts have been made and theoretical models have been proposed,[2–12] there have been little experimental data on the transient species involved in carbon nanotube formation.[9–19] Much of the theory has been inferred from the structure of the carbon nanotubes and from surface examination of the target material.[9–12] Only recently has *in situ* experimental work been reported with regard to nanotube formation. Spectral emission and laser induced fluorescence studies of C_2 during carbon nanotube formation in a laser-produced plume have been performed by Arepalli *et al.*[16,17] Geohegan and co-workers have recently reported *in situ* studies of cobalt which are consistent with this work on nickel.[18,19] However, *in situ* studies of the nickel metal catalyst have been noticeably lacking and are of particular interest since the metal is essential to promotion of nanotube growth. There are several proposals regarding the role of the metal catalyst, from that of the atomic scooter[2] to the role of larger nanometer[6–8] and micrometer sized nickel particles.[3,4] In this work we address the *in situ* monitoring of nickel metal atoms during carbon nanotube formation in a laser-produced plume.

The lack of *in situ* data regarding transient species is due to the difficulty in obtaining spectroscopic information. One of the difficulties in probing metal catalysts during carbon nanotube production by laser ablation is that the carbonaceous emission spectra are so prominent that emission from electronically excited nickel atoms is not detectable. Laser induced fluorescence (LIF) techniques such as laser ablation atomic fluorescence spectroscopy (LAAFS) and laser excited atomic fluorescence spectroscopy (LEAFS) have been shown to be extremely sensitive means of detecting a variety of metals[20–25] including nickel.[26,27] We have made use of LIF to probe nickel atoms during carbon nanotube formation in a laser-produced plume. The work was performed at the Johnson Space Center (JSC) carbon nanotube production lab. The nickel data were evaluated with reference to Arepalli *et al.*'s laser induced fluorescence data on C_2, as well as on C_2 emission spectra and plume diagnostics with respect to lifetimes, temperatures, and plume propagation.[16] The results indicate that the oven temperature is important to promote ablation and long lived plumes which may provide conditions favorable for the chemical interactions of transient species. Initial ablation products are atoms, small molecules, and small clusters with electronic and rotational temperatures much lower than that of the plasma.

II. EXPERIMENT

The nanotube production setup at the Johnson Space Center, described previously by Arepalli *et al.*,[16,17] follows that developed at Rice University.[2] Briefly, the setup includes a carbon target (19 mm in diameter) which is doped with 1% nickel and 1% cobalt and is supported on a rod in an oven which is heated to 1473 K during normal production. The target and rod are centered within a 50.8 mm quartz tube. A smaller 25.4 mm quartz tube is centered within the 50.8 mm tube and extends to within 6 mm of the target. Argon flows through the tubes toward the target at a pressure of 67 kPa and a flow rate of 100 sccm. Two Nd:YAG ablation lasers follow a path through the inner tube and strike the flat end of the target at normal incidence. The green (532

[a)]Electronic mail: garydeboer@letu.edu

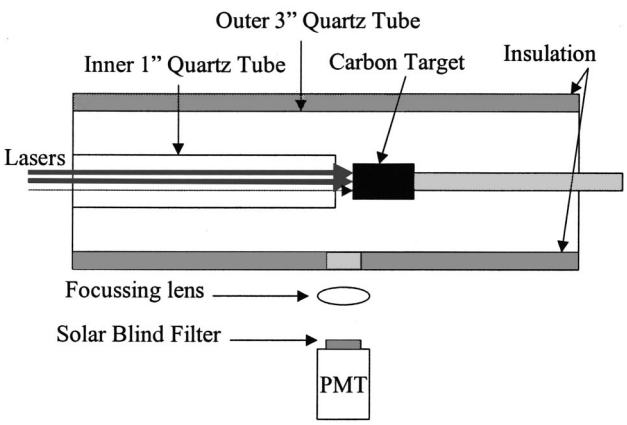

FIG. 1. Carbon nanotube diagnostic setup.

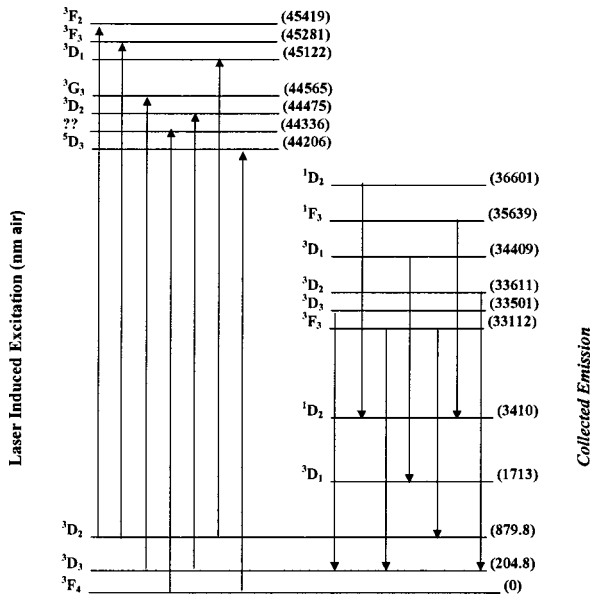

FIG. 2. Transitions involved in the LIF studies of nickel during carbon nanotube formation in a laser-produced plume.

nm) Nd:YAG laser fires 50 ns prior to the IR (1064 nm) Nd:YAG laser. The ablations lasers, which generally operate at 60 Hz, were operated at 10 Hz for these experiments, with an average power output of 1.5 W and an energy density of 1.6 J/cm^2 per pulse for a laser spot size diameter of 3.4 mm. A third Nd:YAG laser (355 nm) operating at 10 Hz is used to pump a Lambda Physik FL 3002 dye laser. The dye (Coumarin 120) laser output was frequency doubled with a BBO1 crystal and was tuned to the atomic lines of nickel over the wavelength range of 224.2–226.2 nm.

Two Stanford Research Systems (SRS) digital delay generators and a 60–10 Hz converter synchronized the lasers. Fluorescence from the metal atoms was focused by a 200 mm focal length lens onto a 1 mm pinhole in front of a Hamamatsu R928 photomultiplier tube (PMT). Fluorescence spectra were acquired by monitoring the PMT signal as a function of dye laser wavelength, laser energies, PMT position, and pump–probe delay. The signals were averaged through a boxcar and the averaged signals were recorded with a personal computer. The time decay of nickel fluorescence was monitored with a LeCroy transient digitizer and a Tektronix digital oscilloscope. Emission was also collected with an optical fiber and a Spex 270M spectrophotometer that was used to resolve the emission. The resolved emission was recorded with an intensified charge coupled device (ICCD).

Wavelengths shorter than 350 nm for excitation and emission of the nickel atom were chosen to avoid spectral interference due to blackbody radiation produced by the oven and carbonaceous emissions resulting from ablation. Also, the PMT is more sensitive in this range. The nature of the production setup results in a great deal of scattered incident radiation from the ablation and probe lasers. To reduce the detection of scattered probe radiation a combination of excitation and fluorescent lines was chosen to allow detection of only the fluorescing radiation. The excitation wavelength was varied from 224.2 and 226.2 nm while collecting fluorescence transitions between 290 and 310 nm. A Solar Blind (SB300) filter centered at 300 nm was placed in front of the PMT, allowing detection of the 300 nm fluorescence, while minimizing the detection of scattered ablation light, scattered dye laser light, and blackbody radiation. A diagram of the diagnostic setup appears in Fig. 1 and an illustration of the transitions involved for excitation and collected fluorescence appears in Fig. 2.

Nickel fluorescence was characterized using a solid nickel target at room temperature. To avoid saturation of the nickel signal a study of the nickel fluorescence signal as a function of laser energy was performed on two different excitation wavelengths. Spectra were also measured at several different dye laser energies to compare the relative intensities of all the electronic transitions within our probed region of 224.2–226.2 nm. The energy studies imply a one photon dependence and that the signal is easily saturated above 100 μJ. In an effort to maintain a linear response of signal intensity to dye laser energy, subsequent fluorescence studies using the nickel target were made with the laser excitation energy less than 100 μJ. The nickel fluorescence signal from ablation of the nickel target was studied as a function of pump–probe time delay and position from the nickel target. Excitation wavelength spectra were taken at several different dye energy outputs and at different pump–probe delays.

The composite production target, composed of approximately 1% nickel and 1% cobalt in graphite, produces carbon deposits on the quartz tubes that diminishes the signal after several minutes of ablation. Expedient data collection became critical when using composite targets. The signal levels for laser induced fluorescence of nickel using these composite targets at 1473 K were comparable to the signal levels obtained from the solid nickel target in spite of the low, 1%, nickel concentration in the composite target. The time delay between ablation lasers was adjusted up to 1 μs, from the nominal 50 ns used for production, and the LIF signal intensity changed very little. Measurements of the nickel LIF signal as a function of dye laser energy at the 224.452 nm resonance indicated much less evidence of saturation than did the nickel signal using the solid nickel target, likely due to changes in ablation and plume propagation. To

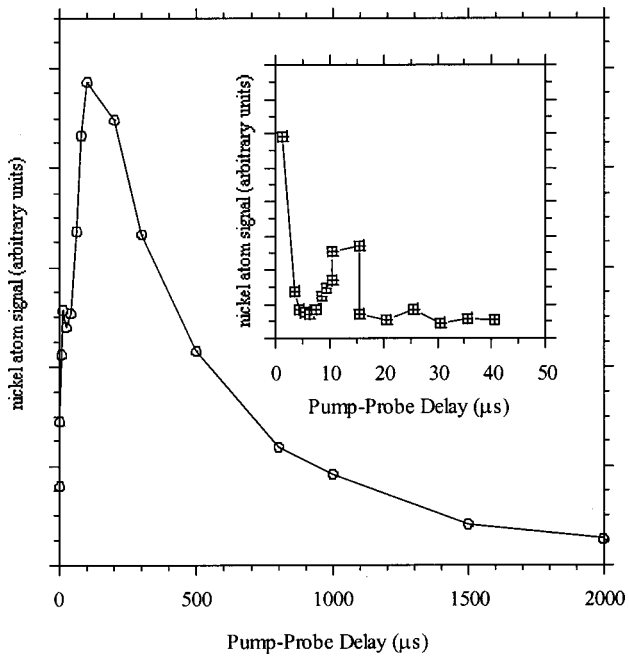

FIG. 3. Nickel signal intensity as a function of pump–probe delay for the composite target at 1453 K and an imaging distance of 1 mm. The inset shows nickel signals for the room temperature nickel target on a shorter time scale. The areas marked ''hot'' and ''cold'' refer to the electronic temperatures at these pump–probe delays.

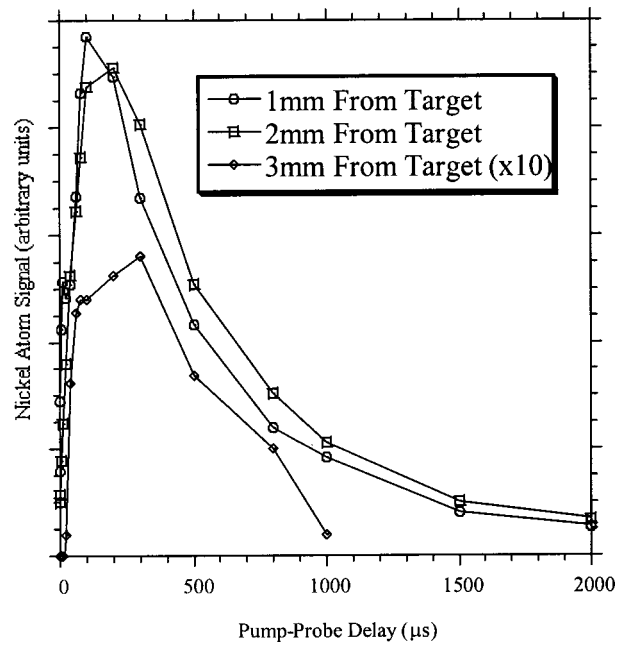

FIG. 4. Nickel atom time profile as a function of imaging distance from the target appearing to show a rate of nickel atom propagation of 10 m/s.

avoid any saturation of the nickel signal using the composite target, dye laser energies were maintained below 100 μJ.

III. RESULTS

A. Nickel atom signal versus pump–probe delay

The transient nickel LIF signal was recorded as a function of the pump–probe delay for the nickel target at room temperature and for the composite target (C:Ni:Co=96:1:1) at 1473 K while positioning the PMT to collect the plume image 1 mm from the target surface, Fig. 3. The nickel signal is seen even when probing within nanoseconds of the second ablation laser, although interference from the ablation lasers make quantifying the nickel fluorescence difficult. The nickel signal originating from the solid nickel target at room temperature soon diminishes, within a few microseconds, then increases only to diminish again within 20 μs of ablation. At an oven temperature of 1473 K the composite target has a pump–probe time profile which appears to be quite different than that for the solid nickel target, resulting in a much longer apparent lifetime of several milliseconds.

Temporal profiles of the hot composite target were also taken at distances of 2 and 3 mm with respect to the target, Fig. 4. The time decay of the apparent nickel LIF signal produced at 1 and 2 mm can be fit to an exponential function. Better fits are obtained using two functions. Half lives are tabulated in Table I. The peak intensities of the 1, 2, and 3 mm profiles suggest that the nickel atoms propagate at a rate of 10 m/s, much slower and with a longer lifetime than reported by Arepalli *et al.* for C_2.[16]

At a peak LIF intensity the PMT signal, imaged 1 mm from the target surface at a pump–probe delay of 200 μs, is proportional to about 2.5 million photons. The transmission of our SB300 filter is approximately 60%. Our spectral window would transmit approximately 10% of the total fluorescence. Assuming the fluorescence is isotropic, we can calculate, based on the dimensions of our system, the fraction of the photons which would have an opportunity to be collected by our lens and focused onto the PMT. The fluorescence originates from the cylinder swept out by the dye laser (2 mm diam) path through the nickel populated portion of the plume. Since the nickel signal is greatly decreased 3 mm from the target surface, let us assume the nickel signal comes from a cylindrical volume 2 mm in diameter and 3 mm in length. At the dye laser wavelength of 224.452 nm, the excitation is from a lower state with energy of 879 cm^{-1}, and thus is only 20% of the total nickel population distributed over the three lowest states (879, 204, and 0 cm^{-1}) at 1500 K. We can then approximate a nickel population density of 10^{14} nickel atoms/cm^3 in the region within 3 mm of the target at a pump–probe delay of 200 μs. With respect to the total amount of material ablated from the target, 3.836×10^{-6} g/pulse, this would imply that nearly all the nickel (1% by weight in the target) would be present within the volume probed. Although the calculation of the nickel atom density is approximate, it would imply that a great deal of

TABLE I. Nickel signal decay rates for the pump–probe profile at 1 and 2 mm with single and two function exponential fits.

Image distance (mm)	Half life (ms) One function	Half life (ms) Two functions
1	372	243, 839
2	372	210, 710

the nickel appears to be in atomic form and is present within a few millimeters of our target surface during the first several hundred microseconds.

B. Plume expansion conditions

Arepalli *et al.* also studied the C_2 emission spectra and the plume expansion during carbon nanotube formation in a laser-produced plume.[16] Plume size, lifetime, and velocity were found to be related to oven temperature and the distance of the target from the inner tube. ICCD images of the plume expansion indicate that under room temperature conditions the expansion is small, short lived, and does travel to within the inner tube. The nickel LIF data seem to indicate similar dependence on oven temperature. The room temperature oven resulted in a short lived nickel atom signal and a small plume, while a hot oven results in a much longer lifetime and greater signal intensity for the nickel atom.

C. Nickel atom LIF spectra

LIF excitation covers a wavelength range of 224.2–226.2 nm and contains eight nickel transitions, of which seven were identified. The unidentified transition is a nickel transition, reported by others in the literature, but its origins are uncertain. It appears to best match a transition from a 204 cm^{-1} lower state. Of the seven identified transitions, three originate from the $^3D_2$ state, two from the $^3D_3$ state, and two from the $^3F_4$ state, with respective energies of 879.816, 204.787, and 0 cm^{-1}. The fluorescence collected when using the SB300 solar blind filter represents fluorescence which occurs not from the excited state directly populated by excitation, but from lower energy excited states (Fig. 2).

Wavelength resolved fluorescence studies done by Axner *et al.*[28] showed a consistent fractional detection of total emission for the lines in our spectral region. We resolved the nickel fluorescence signal excited by the 224.452 and 225.48 nm resonances. A fiber optic introduced the fluorescence into a Spex270 spectrometer that imaged the dispersed fluorescence onto an ICCD. The dispersed fluorescent spectra for these transitions which originate from 879.813 and 0 cm^{-1}, respectively, were very similar, implying that our data should be representative of the excitation intensities for the transitions involved.

If we consider the collected fluorescence signal to be proportional to the absorption intensity, we can infer relative electronic state populations from the line intensities using the transition probability f or line strength S. The application of line strengths is more suited to this analysis. The intensity of a spontaneous emission process in terms of line strength, is

$$I=\{(64\pi^4\nu_{ul}^4/3c^2)\exp[-hcE_u/(kT)]/Q\}S_{ul}, \qquad (1)$$

where ν is the frequency of the transition, E_u is the energy of the upper state, k is the Boltzmann constant, T the temperature in kelvin, Q the partition function, and S_{ul} the line strength factor for the emission from the upper to the lower energy state. The change in ν over our spectral region affects the intensity by only a few percent, so that the first term is relatively constant. The exponential term reflects the populations of the various energy levels, N_i. Equation (1) can then be approximated by

$$I \propto N_i S_{ul}. \qquad (2)$$

Relative populations can be found by dividing the transition intensity by the line strength factor. Given the relative population, this population can be fit as a function of its electronic energy to a Boltzmann distribution, Eq. (3), to obtain an electronic temperature,

$$N_i/N_0 = e^{-\Delta E/kT}, \qquad (3)$$

where ΔE is the respective energy of each electronic state relative to the ground state.

Spectra were corrected for variations in laser excitation energy by dividing the raw LIF data with the product of the measured dye laser energy times the wavelength, $E = Nhc/\lambda$, such that N, the number of photons, is proportional to $E\lambda$. The wavelength factor affects the spectra minimally, since the change in wavelength is less than 1% over our spectral region.

In Fig. 5 each line of the energy normalized spectra was integrated and the baseline corrected. These integrated intensities were then divided by the respective line strength factor to obtain relative electronic state populations. Electronic temperatures obtained in this manner range from 1000 to 2000 K. A synthetic spectrum[29] for a temperature of 1500 K is compared to experiment in Fig. 5.

It should be noted that the 1500 K temperature fit is a minimal temperature needed to obtain a fit. Temperatures higher than 1500 K do not change the synthetic spectrum to any great extent because the dependence of populations is

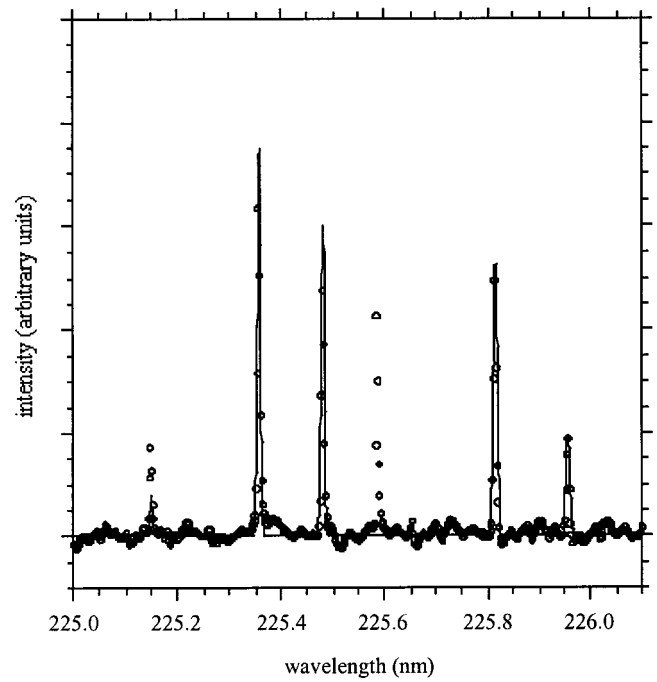

FIG. 5. Nickel spectra taken with a room temperature nickel target compared with a 1500 K synthetic spectrum. Note that the transition at 225.58? nm is an unidentified transition.

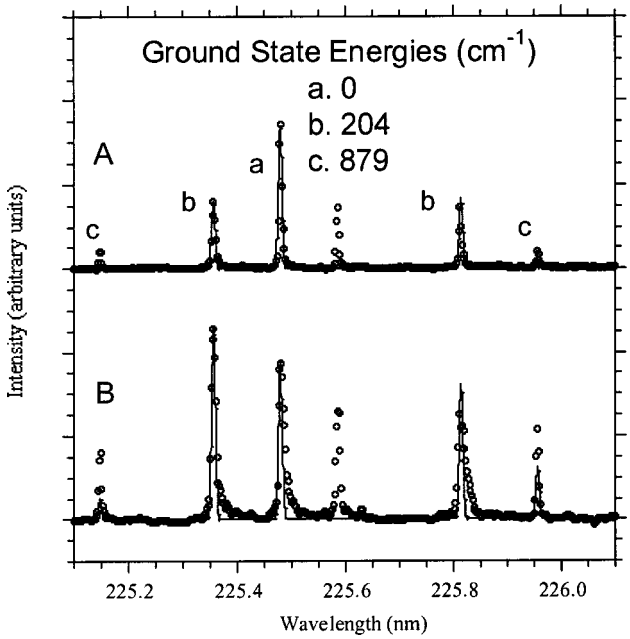

FIG. 6. Spectra taken with a room temperature nickel target at (A) 24 and (B) 8 ms delay with respect to the pump probe. The spectrum in (A) is fit with a temperature of 275 K, while that in (B) is fit with a temperature of 1500 K.

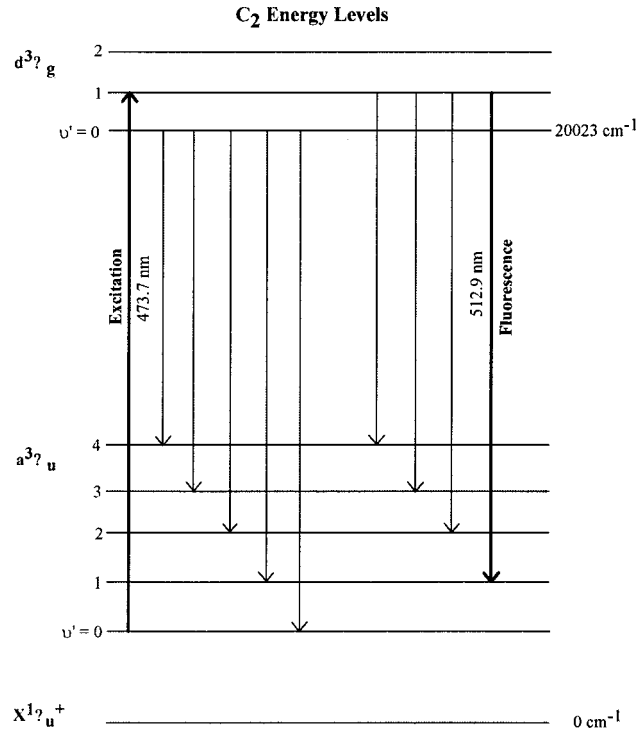

FIG. 8. Transitions involved in the LIF studies of C_2 during carbon nanotube formation in a laser-produced plume.

less sensitive at higher temperatures. The actual temperature of the spectra may be as low as 1000 K but could be much greater than 1500 K.

Spectral data were also compared within an experimental day as a function of pump–probe delay. Two of these spectra taken with the nickel target at room temperature appear in Fig. 6 along with synthetic spectra. Temperatures obtained from these spectra are 275 K for the 24 μs delay and 1500 K for the 8 μs delay. It is clearly seen that there is an increase in intensity for the lower energy states at a later pump–probe delay. When using the composite target at 1473 K, Fig. 7, it is seen that the later pump–probe delay of 200 μs exhibits a warmer spectrum than does the earlier delay of 10 μs. For both the hot composite target and the room temperature solid nickel target (Figs. 7 and 8) the warmer spectra relate to greater nickel signal intensity within the temporal pump–probe profile while the cooler spectra correspond to a lesser nickel signal intensity. It should be noted that the spectra obtained from the room temperature nickel target and those from the oven heated composite target can both be fit to a synthetic spectrum with a temperature of 1500 K.

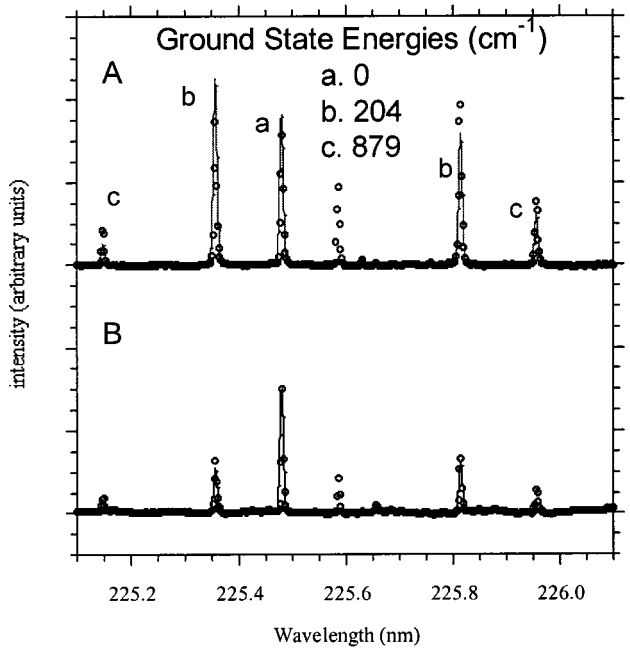

FIG. 7. Nickel spectra taken with a Ni/Co/C target at a temperature of 1473 K at (A) 200 and (B) 10 μs. The spectrum with the earlier delay appears cooler, 225 K, than the later spectrum, 1500 K. This is in contrast to the results obtained with the room temperature nickel target.

D. Rotational temperature fitting of C_2 spectra by line strength analysis

Arepalli *et al.*[16] reported laser induced fluorescence data for C_2. Additional analysis of that data is reported here to complement the nickel fluorescence data. The C_2 spectra represent a single electronic and a single vibrational transition but many different rotational energy transitions. The spectral region of 473–474 nm corresponds to the 0-1 transition from the $a^3\Pi_u$ to the $d^3\Pi_g$ electronic state. A diagram of the C_2 Swan band for the 0-1 transition appears in Fig. 8. The spectral region probed consists almost entirely of the *P* branch of the rotational spectrum with only a small contribution from the *Q* and *R* branches. The experimental spectra were fit to synthetic spectra, similar to the method described for nickel.[29] A calculated spectrum, for rotational temperature of 400 K, illustrating the three branches of the spectrum is seen in Fig. 9. An example of the fits appears in Fig. 10 and the

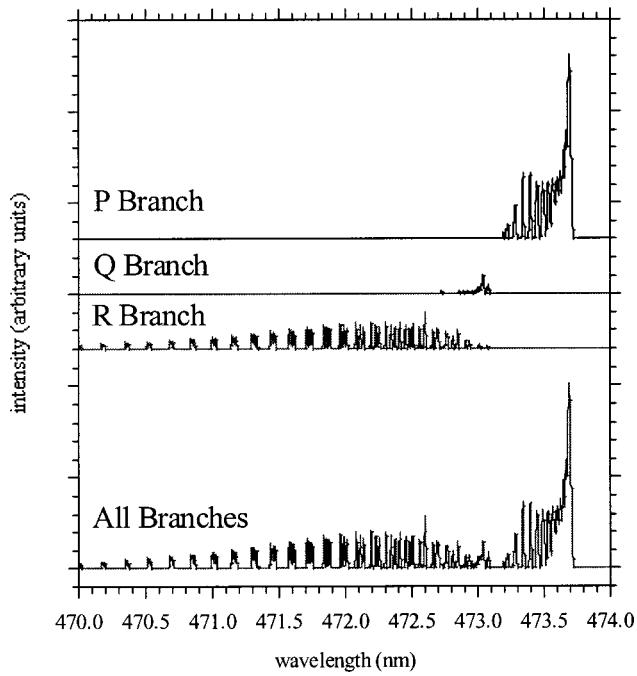

FIG. 9. Synthetic C_2 spectra at 400 K that demonstrate the *P*, *Q*, and *R* branches of the rotational–vibrational transition of the 0-1 Swan band.

resulting temperatures appear in Table II. Arepalli *et al.* measured the bandhead intensities of the C_2 spectra as a function of pump–probe delay.[16] As with the nickel data, higher temperatures are associated with the more intense signal.

These temperatures are regarded as maxima, since higher temperatures result in increased intensity to *P*, branch transitions in the 473.1–473.2 nm range which is not evidenced in the spectra in Fig. 11. Also, the ratio of the bandhead intensity at 473.69 nm to the 473.34 or 473.40 nm

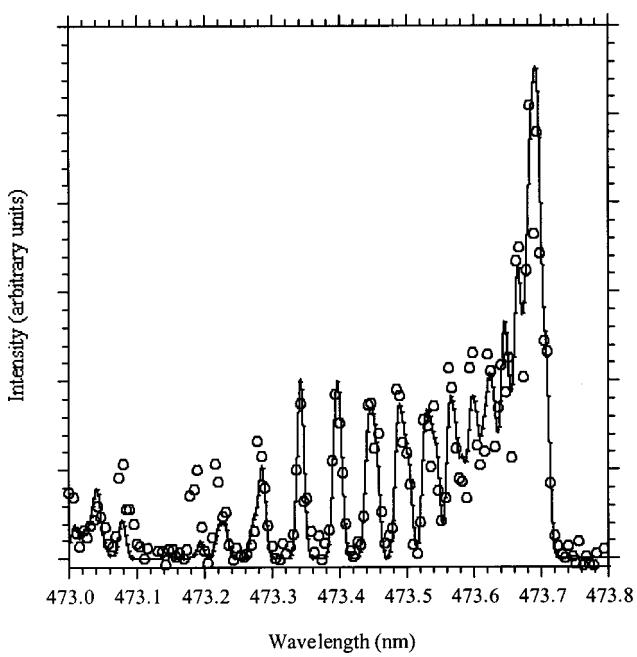

FIG. 10. C_2 spectra taken at a 20 μs delay and at an imaging distance of 1.775 mm fit to a temperature of 400 K.

TABLE II. Rotational temperatures for C_2 as a function of pump–probe delay and image position.

Delay (μs)	Distance (mm)	Temperature (K)	Intensity
1	−0.225	350	
1	0.775	350	
1	1.775	400	
1	1.775	400	
1	2.775	700	
1	4.775	300	
0.25	1.775	350	4.5
5	1.775	400	6
20	1.775	400	2
40	1.775	350	0.25

transitions continues to increase up to about 600 K. The experimental ratio is much less than the ratio at 600 K, indicating a lower rotational temperature. The rotational temperatures and bandhead intensities as a function of laser pump–probe delay are plotted in Fig. 12. Figure 13 illustrates the relationship between the C_2 rotational temperature and the imaging position. It should also be noted that the C_2 data were taken using only the IR laser for ablation, while the nickel data were taken using both the IR laser and the green laser for ablation. The use of only the IR laser is likely responsible for the lower C_2 temperatures. Carbon nanotubes do form when the IR laser is used without the 532 nm laser, but with less of a yield.

IV. DISCUSSION

Since metal catalysts are essential to carbon nanotube formation, several studies have focused on the behavior of the metal. Yudasaka *et al.*[11] have shown, by inspection of targets, that when Nd:YAG pulsed lasers are used there is poor metal ablation at room temperature and carbon nano-

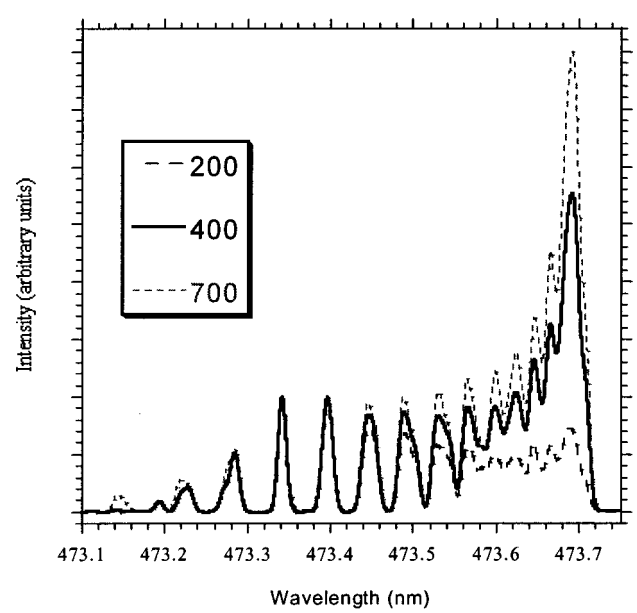

FIG. 11. Synthetic C_2 spectra at 400, 500, 600, and 700 K. Note the change in the bandhead intensity and the growth in the *P* branch transition at 473.15 nm.

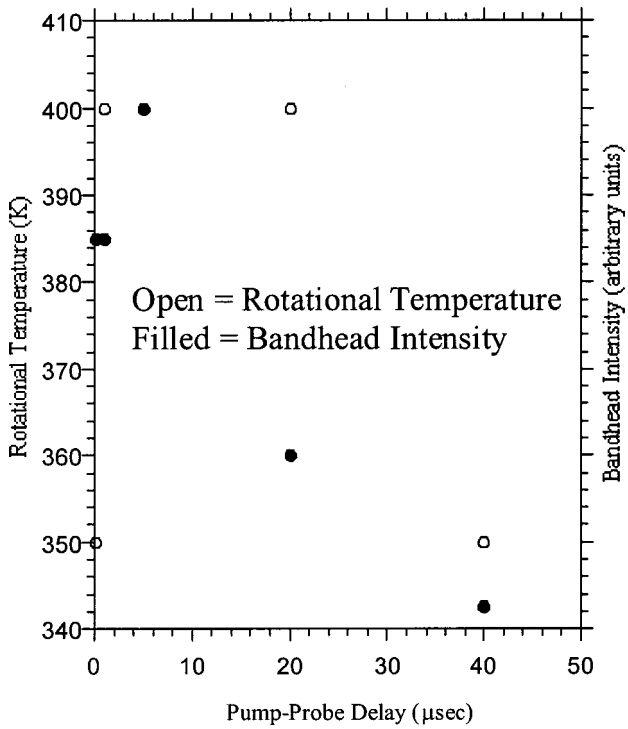

FIG. 12. C_2 rotational temperature and bandhead intensities at an imaging distance of 1.775 mm vs pump–probe delay.

tubes do not form. However, when the target is heated to 1473 K carbon nanotubes do form and the metal is ablated from the target. Yudasaka *et al.* also noted that when a CO_2 laser is used at room temperature carbon nanotubes are also formed, implying that the elevated ambient gas medium temperature is not necessary for nanotube assembly, but, rather, for metal ablation.[10] The millisecond CO_2 laser has a much longer pulse than the nanosecond Nd:Yag or excimer lasers.

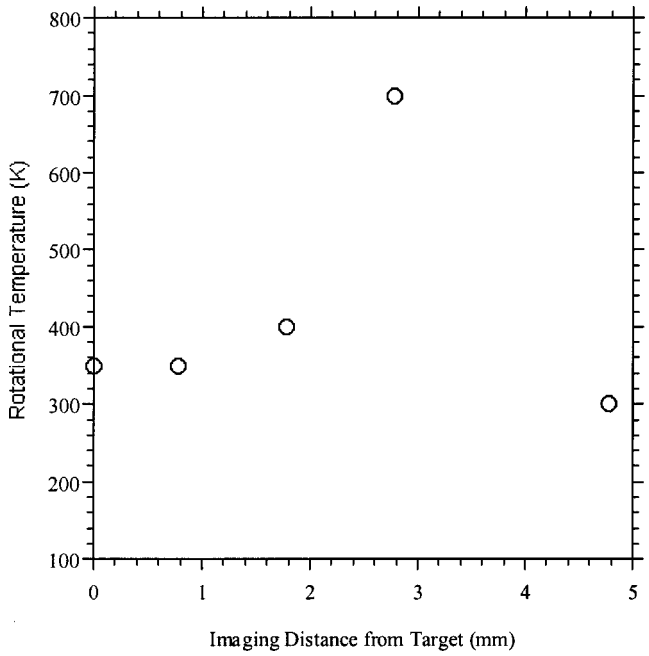

FIG. 13. C_2 rotational temperature vs imaging position at a pump–probe delay of 1 μs.

It is possible that the longer heating time of the CO_2 laser allows better ablation so that elevated oven temperatures are not necessary. This work is consistent with an increase in nickel metal ablation at elevated oven temperatures. This work also indicates that the electronic temperature of nickel atoms produced by laser ablation is at least 1500 K in the center of the plume regardless of the oven temperature and becomes much lower outside of the plume. The propagation and the lifetime of nickel atoms clearly change when the oven is used to elevate the target temperature.

Temperatures obtained from the nickel and carbon LIF spectra are much cooler than those indicated by the C_2 emission. Similar LIF and emission studies done by Brinkman *et al.*[30] in a dc arcjet for purposes of analyzing diamond deposition found similar temperature differences between C_2 emission and LIF. Temperature measurements based on a variety of methods in other systems appear to give similar temperature variations for the electronically excited state and ground state species.[31–35] Brinkman *et al.* postulated that the quenching of the excited electronic C_2 species is much faster than a multiple collision process necessary for reaching vibrational and rotational thermal equilibrium. The hot C_2 emission has a lifetime of about 60 μs, implying that during this time short lived C_2 species are being formed.

Laser produced plumes associated with carbon have been studied.[36–38] These studies indicate that the carbonaceous emission results primarily from recombination of atomic carbon to produce hot C_2 emission spectra. Arepalli *et al.*[39] have also explored the possibility that C_2 emission can result from the photodissociation or ''shrinkage'' of fullerenes. Both of these sources, and possibly others, are likely contributors to the hot C_2 emissions.

Computational studies based on analysis of the endcaps of carbon nanotubes formed in the dc arc indicate that the growth of carbon nanotubes occurs at between 700 and 1800 K, rather than at the much higher temperatures of the plasma.[9] The dependence of the nanotube diameter on the oven temperature would also indicate that oven temperatures have a role in the formation process.[40] Arepalli *et al.*[16] have shown that the oven temperature influences the plume propagation, size, and lifetime when Nd:YAG lasers are used for ablation. They have also shown that the target position relative to that of the inner tube can affect the plume propagation. The empirically determined optimal target position for the formation of carbon nanotubes also relates to the position in which the plume appears to have the slowest rate of propagation. No doubt the distance of the target from the inner tuber influences the argon gas flow characteristics around the target. Yudasaka *et al.*[12] also noted that nickel ablation has a gas pressure dependency, although they attributed this dependency to effects of ablation rather than of plume propagation. The ablation process influences the propagation of the plume very much and so it is difficult to analyze them independent of each other.

With regard to whether the metal species within the plume are atomic or large micrometer sized particles or melts, various work to characterize plumes produced by laser ablation can be elucidative.[36–38,41–45] Plume associated metals, including nickel, have been studied.[42–45] In general, it

has been found that higher laser energy densities and gas pressures appear to be necessary to create metallic nanoparticles or liquid droplets by laser ablation.[42–44] Given the conditions of our experiments it seems likely that the initial ablation results in atomic and small molecular species than in the larger particles and droplets being less prevalent.

Dillon *et al.*[46] have addressed the specific question of carbon nanotube formation as a function of laser parameters. They studied the formation of carbon nanotubes using pulsed lasers at 3–24 kHz with various pulse energies and continuous wave lasers. They indicated that tubes are formed at higher laser powers, but with lower pulse energies and higher pulse frequency, consistent with smaller species being ablated. This implies that the formation of carbon nanotubes is favored by species that are in the vapor phase.

Lifetimes of the C_2 and nickel atoms reported in this work may indicate that nickel atoms are more prevalent than nickel particles or droplets. The long lifetime of the nickel atom signal, which peaks at about 100 μs and then appears to decreases according to a biexponential function with half lives of about 230 and 780 μs, would suggest that the presence of the atomic species is more prevalent than nickel particles or droplets for the first several hundred microseconds. Lifetime emission and LIF of C_2 are shorter than the lifetime of the nickel LIF signal which may indicate that the nucleation process for carbon is faster than it is for the nickel metal. Geohegan and co-workers observed a similarly long lifetime for the cobalt atom,[18] consistent with the suggestion that more metal atoms rather than metal clusters or particles are present during the first several milliseconds after ablation.

Maiti *et al.* reported experimental nanotube growth rates of 1–500 Å/ms for the dc arc process and calculated a growth rate of 8.2×10^2 Å/ms at 1500 K and 1.9×10^4 Å/ms at 2000 K based on molecular dynamics simulations.[6] This would imply a growth time of one to many milliseconds for a micron long tube. Smalley[47] and Scott *et al.*[48] proposed much shorter, microsecond times for nanotube formation during laser ablation, while other groups, such as Puretzky *et al.*,[19] Kokai *et al.*,[13,14] and Gorbunov,[49] proposed formation times of as long as seconds. Time scales on the order of milliseconds and longer would allow metal nucleation during nanotube formation. The nucleation of metals into small bimetallic clusters may be the reason for a bimetallic dependence of the metal catalyst. Clearly, additional efforts to determine the growth rates of nanotubes and the presence of nanotubes during the formation process are necessary.

V. CONCLUSION

This work demonstrates that the nickel metal catalyst can be monitored *in situ* during carbon nanotube formation. Elevation of the oven temperature increases the amount of ablation and also appears to influence plume expansion and propagation. The distribution of energies in the nickel atom and the rotational energies of the ground electronic state of the C_2 species inferred from the LIF spectra imply that the temperatures of these species are much lower than the plasma temperature. The temperatures determined by LIF are more closely related to the ambient oven temperature. The laser power densities, gas pressures, as well as metal and C_2 lifetimes are consistent with an atomic or small molecule presence upon ablation. Additional experiments including LIF studies of C_2 using two ablation lasers, additional LIF studies of nickel and cobalt as a function of various system parameters, and an *in situ* method to monitor nanotube growth would be beneficial to this work.

ACKNOWLEDGMENT

The authors acknowledge the financial support of NASA under Grant No. NAS9-19100 and NAG 9-1174. Assistance from Tom Leimkuehler and Jim Hornkohl for the initial C2 data collection and analysis is acknowledged. GDB appreciates the support from the NASA-JSC Summer Faculty Fellowship Program.

[1] S. Iijima, Nature (London) **354**, 56 (1991).
[2] R. E. Smalley *et al.*, Science **273**, 483 (1996).
[3] R. S. Ruoff, D. C. Lorents, and R. Malhotra, Nature (London) **366**, 637 (1993).
[4] A. Maiti, C. J. Brabec, and J. Bernholc, Phys. Rev. B **55**, R6097 (1997).
[5] C. Kiang, W. A. Goddard, R. Beyers, J. R. Salem, and D. S. Bethune, Mater. Res. Soc. Symp. Proc. **359**, 69 (1995).
[6] A. Maiti, C. J. Brabec, C. Ronald, and J. Bernholc, Phys. Rev. B **52**, 14850 (1995).
[7] A. Fonseca, K. Hernadi, P. Piedigrosso, L. P. Biro, S. D. Lazarescu, P. Lambin, P. A. Thiry, D. Bernaerts, and J. B. Nagy, *Proceedings of Fullerenes: Chemistry of Physics and New Directions IX* (The Electrochemistry Society, Montreal, 1997).
[8] M. Yudasaka, T. Ichihashi, T. Komatsu, and S. Iijima, J. Phys. Chem. **102**, 4892 (1998).
[9] V. H. Crespi, Phys. Rev. Lett. **82**, 2908 (1998).
[10] M. Yudasaka, S. Iijima, F. Kokal, K. Takahashi, R. Yamada, N. Sensui, and T. Ichihashi, J. Phys. Chem. **103**, 3576 (1999).
[11] M. Yudasaka, R. Kikuchi, O. Yoshimasa, O. Etsuro, and S. Yoshimura, Appl. Phys. Lett. **70**, 1817 (1997).
[12] M. Yudasaka, T. Komatsu, Y. Ichihashi, Y. Achiba, and S. Iijima, J. Phys. Chem. B **102**, 4892 (1998).
[13] F. Kokai, K. Takahashi, M. Yudasaka, and S. Iijima, Appl. Phys. A: Mater. Sci. Process. **A69**, S229 (1999).
[14] F. Kokai, K. Takahashi, and M. Yudasaka, J. Phys. Chem. B **103**, 4346 (1999).
[15] F. Kokai, K. Takahashi, and M. Yudasaka, J. Phys. Chem. B **104**, 6777 (2000).
[16] S. Arepalli, P. Nikolaev, W. Holmes, and C. D. Scott, Appl. Phys. A: Mater. Sci. Process. **A70**, 125 (2000).
[17] S. Arepalli and C. D. Scott, Chem. Phys. Lett. **302**, 139 (1998).
[18] A. A. Puretzky, D. B. Geohegan, X. Fan, and S. J. Pennycook, Appl. Phys. Lett. **76**, 182 (2000).
[19] A. A. Puretzky, D. B. Geohegan, X. Fan, and S. J. Pennycook, Appl. Phys. A: Mater. Sci. Process. **A70**, 153 (2000).
[20] W. Sdorra and K. Niemax, Inst. Phys. Conf. Ser. **11**, 463 (1990).
[21] Y. Oky, T. Tani, N. Kidera, and M. Maeda, Opt. Commun. **110**, 298 (1994).
[22] J. D. Winefordner, S. J. Weeks, and H. Haraguchi, Anal. Chem. **50**, 360 (1978).
[23] R. G. Michel, J. X. Zhou, X. Hou, and S.-J. J. Tsai, Anal. Chem. **69**, 490 (1997).
[24] R. G. Michel, J. P. Dougherty, and F. R. Preli, J. Anal. At. Spectrom. **2**, 429 (1987).
[25] M. Maeda, Y. Oki, and E. Tashiro, Anal. Chem. **65**, 2096 (1993).
[26] J. D. Winfordner, M. S. Epstein, J. Bradshaw, S. Bayer, J. Bower, and E. Voigtman, Appl. Spectrosc. **34**, 372–376 (1980).
[27] O. Axner, A. Marunkov, N. Cherkalin, and J. Enger, Spectrochim. Acta B **49**, 1385 (1994).
[28] O. Axner, A. Marunkov, N. Chekalin, and J. Enger, Spectrochim. Acta B **49**, 1385 (1994).
[29] J. Hornkohl (Tennessee Space Institute, Tullahoma, Tennessee).

[30] E. A. Brinkman, G. A. Ralche, M. S. Brown, and J. B. Jeffries, Appl. Phys. B: Lasers Opt. **B64**, 689 (1996).
[31] J. A. Pobst, I. J. Wysong, and R. A. Spores, IEPC **95**, 203 (1995).
[32] G. A. Raiche and J. B. Jeffries, Appl. Opt. **32**, 4629 (1993).
[33] A. G. Gaydon, *The Spectroscopy of Flames*, 2nd ed. (Haisted, New York, 1974).
[34] R. P. Van Ingen, J. Appl. Phys. **76**, 8065 (1994).
[35] R. P. Van Ingen, J. Appl. Phys. **76**, 8055 (1994).
[36] C. Parigger, D. H. Plemmons, J. O. Hornkohl, and J. W. L. Lewis, J. Quant. Spectrosc. Radiat. Transf. **52**, 707 (1994).
[37] S. I. Aoqui, T. Ikegami, Y. Yamagaa, and K. Ebihara, Thin Solid Films **316**, 40 (1998).
[38] J. Seth, R. Padiyath, and S. V. Babu, Appl. Phys. Lett. **63**, 126 (1993).
[39] S. Arepalli, C. D. Scott, P. Nikolaev, and R. E. Smalley, Chem. Phys. Lett. **320**, 26 (2000).
[40] S. Bandow, S. Asaka, Y. Saito, A. M. Rao, L. Grigorian, E. Richter, and P. C. Eklund, Phys. Rev. Lett. **80**, 3779 (1998).
[41] C. Miller, *Laser Ablation Principles and Applications* (Springer, Berlin, 1994).
[42] M. F. Becker, J. R. Brock, H. Cai, D. E. Henneke, J. W. Keto, J. Lee, W. T. Nichols, and H. D. Glicksman, Nanostruct. Mater. **10**, 853 (1998).
[43] K. H. Song and X. Xu, Appl. Surf. Sci. **127–129**, 111 (1998).
[44] J. A. Aguilera, C. Aragon, and F. Penalba, Appl. Surf. Sci. **127–129**, 309 (1998).
[45] M. Tanaka, Y. Fujisawa, T. Nakajima, Y. Tasaka, and K. Ota, J. Appl. Phys. **83**, 3379 (1998).
[46] A. C. Dillon, P. A. Parilla, K. M. Jones, G. Riker, and M. J. Heben, Adv. Laser Abl. Mater. (USA) **526**, 403 (1998).
[47] R. E. Smalley, Acc. Chem. Res. **25**, 98 (1992).
[48] C. D. Scott, S. Arepalli, P. Nikalaev, and R. Smalley (unpublished).
[49] A. A. Gorbunov, Appl. Phys. A: Mater. Sci. Process. **A69**, S593 (1999).